Experimental Section

Synthesis of $NiFe_2O_4$/RGO

All the chemicals are of analytical grade and used as received. $NiFe_2O_4$/RGO was synthesized by a facile microwave-assisted hydrothermal method. Typically, 20 mg of GO was dispersed in 30 mL of deionized water under ultrasonic dispersion for 1 h. Then, 0.1 mmol of $Ni(NO_3)_2 \cdot 6H_2O$ and 0.2 mmol of $Fe(NO_3)_3 \cdot 9H_2O$ were co-added in the GO suspension under magnetic stirring to form a homogeneous solution. The mixture was sealed into a quartz vial, and irradiated in a microwave oven (2450 MHz) for 10 min, and then cooled to room temperature naturally. The product was collected by centrifugation and then washed several times with deionized water and then dried at 60°C for 12 h. The dried precipitates were placed into a horizontal quartz tube and heated to 600 °C for 2 h under Ar atmosphere to obtain $NiFe_2O_4$/RGO. For comparison, RGO were prepared by the same procedure without addition of $Ni(NO_3)_2 \cdot 6H_2O$ and 0.2 mmol of $Fe(NO_3)_3 \cdot 9H_2O$. For comparison, pure $NiFe_2O_4$ and pure RGO were prepared by the same procedure as $NiFe_2O_4$/RGO without the addition of GO and $Ni(NO_3)_2 \cdot 6H_2O$/$Fe(NO_3)_3 \cdot 9H_2O$, respectively.

Electrochemical experiments

The electrochemical measurements were performed on a CHI-660 electrochemical workstation (CHI-660) in a three-electrode configuration, where carbon cloth (CC), Ag/AgCl electrode and graphite rod were used as working, reference and counter electrodes, respectively. The working electrode was prepared by the following process: 100 μl of the homogeneous ink prepared by dispersing 1 mg catalyst and 5 μL of Nafion (5 wt%) in 95 μL of ethyl alcohol. Then 20 μL of catalyst ink was loaded on a 1×1 cm^2 CC substrate and dried under ambient condition. All potentials were referenced to reversible hydrogen electrode (RHE) by following equation: E_{RHE} (V)=$E_{Ag/AgCl}$+0.197+0.059×pH. Potentiostatic test was conducted in N_2-saturated 0.5 M $LiClO_4$ solution in a two-compartment cell, which was separated by Nafion 211 membrane. The Nafion membrane was pretreated by boiling it in 5% H_2O_2 solution for 1 h, 0.5 M H_2SO_4 for 1 h and deionized water for 1 h in turn. Prior

to electrolysis, the feeding gases were purified through 0.05 M H_2SO_4 solution to remove any possible contaminants (NH_3 and NO_x). During each electrolysis, ultra-high-purity N_2 gas (99.999%) was continuously purged into the cathodic chamber at a flow rate of 20 mL min^{-1}. After each NRR electrolysis, the produced NH_3 and possible N_2H_4 were quantitatively determined by the indophenol blue method[1], and approach of Watt and Chrisp[2], respectively.

Determination of NH_3

4 mL of electrolyte was removed from the electrochemical reaction vessel. Then 50 μL of solution containing NaOH (0.75 M) and NaClO (ρ_{Cl} = ~4), 500 μL of solution containing 0.32 M NaOH, 0.4 M $C_7H_6O_3$, and 50 μL of $C_5FeN_6Na_2O$ solution (1 wt%) were respectively added into the electrolyte. After standing for 2 h, the UV-Vis absorption spectrum was measured and the concentration-absorbance curves were calibrated by the standard NH_4Cl solution with a series of concentrations.

$$\text{NH}_3 \text{ yield } (\mu\text{g h}^{-1} \text{ mg}_{\text{cat.}}^{-1}) = \frac{c_{\text{NH}_3} \times V}{t \times m} \quad (1)$$

Faradaic efficiency was calculated by the following equation:

$$\text{Faradaic efficiency } (\%) = \frac{3 \times F \times c_{\text{NH}_3} \times V}{17 \times Q} \times 100\% \quad (2)$$

where c_{NH3} (μg mL^{-1}) is the measured NH_3 concentration, V (mL) is the volume of the electrolyte, t (h) is the reduction time and m (mg) is the mass loading of the catalyst on CC. F (96500 C mol^{-1}) is the Faraday constant, Q (C) is the quantity of applied electricity.

Determination of N_2H_4

5 mL of electrolyte was removed from the electrochemical reaction vessel. The 330 mL of color reagent containing 300 mL of ethyl alcohol, 5.99 g of $C_9H_{11}NO$ and 30 mL of HCl were prepared, and 5 mL of color reagent was added into the electrolyte. After stirring for 10 min, the UV-Vis absorption spectrum was measured and the concentration-absorbance curves were calibrated by the standard N_2H_4 solution with a series of concentrations.

Nuclear magnetic resonance measurement

^{1}H nuclear magnetic resonance (NMR) measurement was carried out using $^{15}N_2$ (99 % isotopic purity) as the feed gas. Prior to NMR measurement, $^{15}N_2$ was purified by an acid trap (0.05 M H_2SO_4) to eliminate the NO_x and NH_3 contaminants [4]. The NRR experiment using $^{15}N_2$ was conducted for 2 h. After NRR electrolysis, 4 mL of electrolyte was removed from the electrochemical reaction vessel, which was concentrated to ~1 mL and further acidized to pH ~2. The obtained electrolyte was mixed with 0.1 mL of deuterium oxide (D_2O) containing 100 ppm of dimethyl sulphoxide (DMSO) and 70 μL of D_2O for NMR spectroscopy measurement (500 MHz Bruker superconducting-magnet NMR spectrometer).

Characterizations

X-ray diffraction (XRD) pattern was tested on a Rigaku D/max 2400 diffractometer. Transmission electron microscopy (TEM), high-resolution transmission electron microscopy (HRTEM) and scanning transmission electron microscopy (STEM) were performed on a Tecnai G^2 F20 microscope. Raman spectra were recorded on a JY-HR800 Raman spectroscope. The UV-vis absorbance measurements were performed on a MAPADA P5 spectrophotometer.

Calculation details

Density functional theory (DFT) calculations were carried out using the Cambridge sequential total energy package (CASTEP) code. The exchange-correlation interaction was described by generalized gradient approximation (GGA) with the Perdew-Burke-Ernzerhof (PBE) functional. An effective *U* parameter of 5.0 eV was applied for Fe 3d states, while 6.5 eV was used for Ni 3d states. During the geometry optimization, the Monkhorst-Pack k-point mesh and energy cutoff were set to be 2×2×1 k-points and 400 eV. The $NiFe_2O_4$ (311) surface was modeled by a (2×2) supercell. For the construction of surface models, a vacuum of 15 Å was used to eliminate interactions between periodic images.

The adsorption energy (ΔE) was calculated by the following equation[4]:

$$\Delta E = E_{ads/slab} - E_{ads} - E_{slab} \quad (3)$$

where $E_{ads/slab}$, E_{ads} and E_{slab} are the total energies for adsorbed species on slab,

adsorbed species and isolated slab, respectively.

The Gibbs free energy (ΔG) of the NRR intermediates is calculated as [4]:

$$\Delta G=\Delta E+\Delta ZPE-T\Delta S \quad (4)$$

where ΔE is the adsorption energy, ΔZPE is the zero point energy difference and $T\Delta S$ is the entropy difference between the gas phase and adsorbed state.

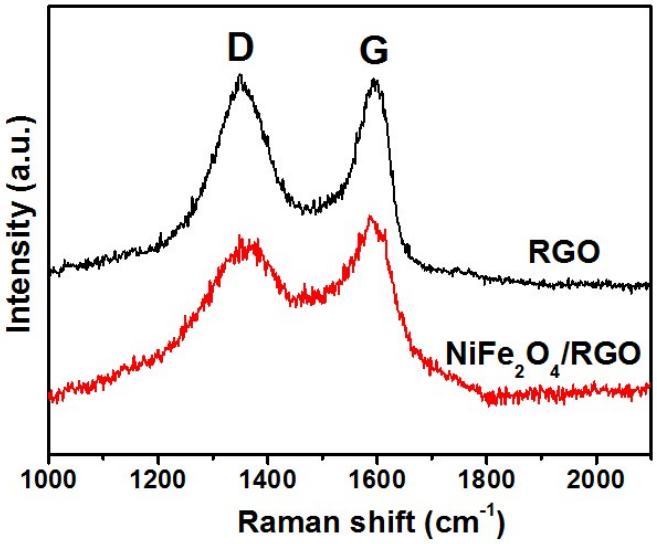

Fig. S1. Raman spectra of $NiFe_2O_4$/RGO.

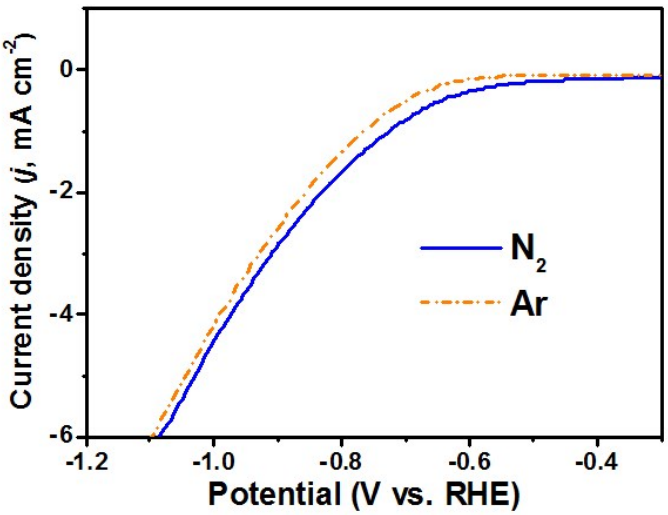

Fig. S2. LSV curves of $NiFe_2O_4$/RGO in Ar- and N_2- saturated solutions.

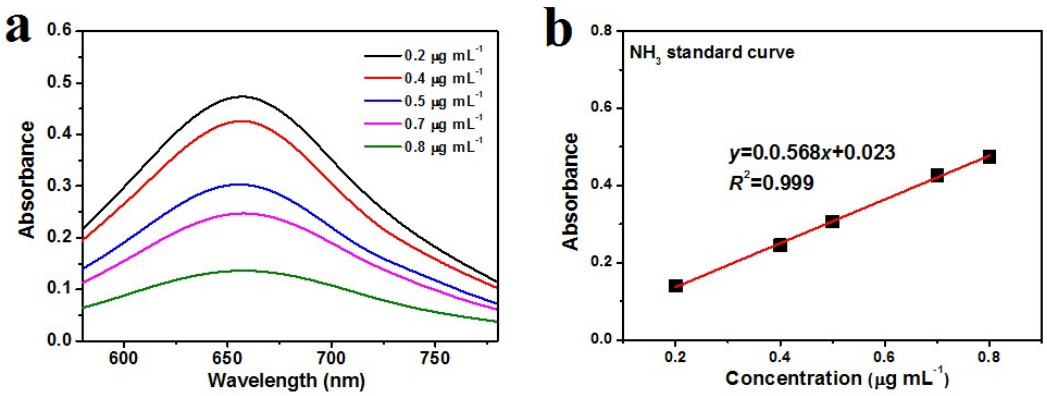

Fig. S3. (a) UV-Vis absorption spectra of indophenol assays with NH_4Cl after incubated for 2 h at ambient conditions. (b) Calibration curve used for calculation of NH_3 concentrations.

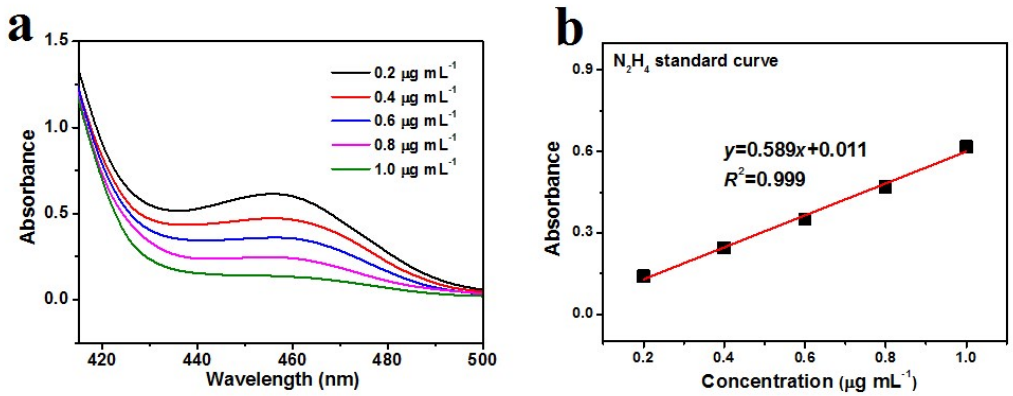

Fig. S4. (a) UV-Vis absorption spectra of N_2H_4 assays after incubated for 20 min at ambient conditions. (b) Calibration curve used for calculation of N_2H_4 concentrations.

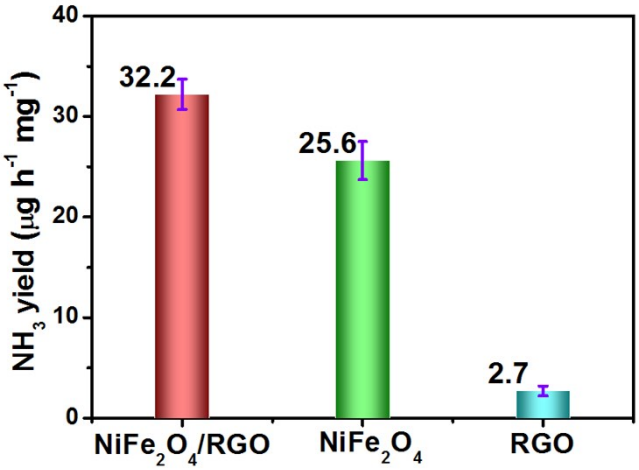

Fig. S5. NH_3 yields of $NiFe_2O_4$/RGO, $NiFe_2O_4$ and RGO after 2 h of NRR electrolysis at -0.5 V. The pure $NiFe_2O_4$ and pure RGO were prepared by the same procedure as $NiFe_2O_4$/RGO without the addition of GO and $Ni(NO_3)_2 \cdot 6H_2O$/$Fe(NO_3)_3 \cdot 9H_2O$, respectively.

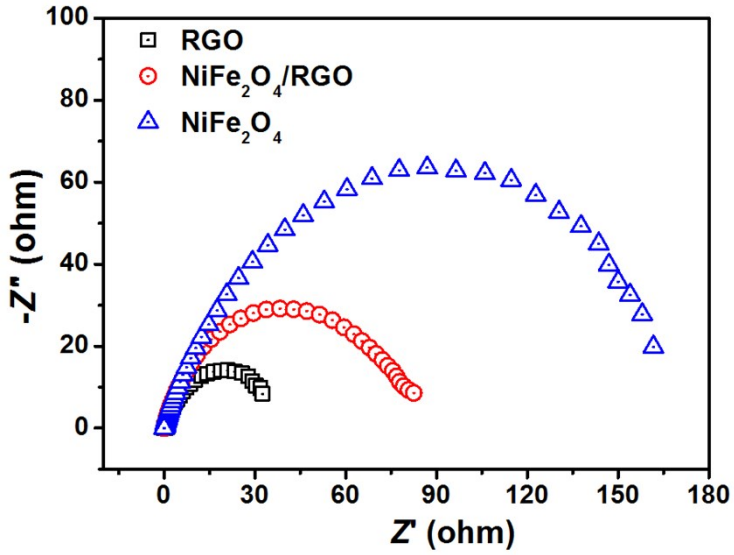

Fig. S6. Electrochemical impendence spectra of $NiFe_2O_4$/RGO, $NiFe_2O_4$ and RGO.

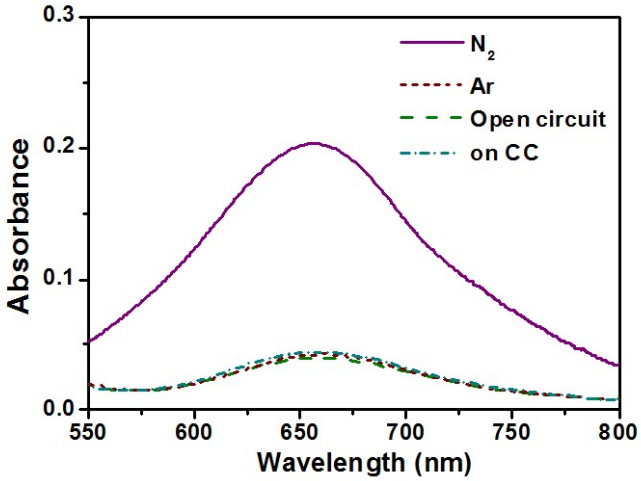

Fig. S7. UV-Vis absorption spectra of the electrolytes stained with indophenol indicator after 2 h electrolysis on $NiFe_2O_4$/RGO at -0.5 V in N_2-saturated solution, Ar-saturated solutions, N_2-saturated solution at open circuit and N_2-saturated solution on pristine CC.

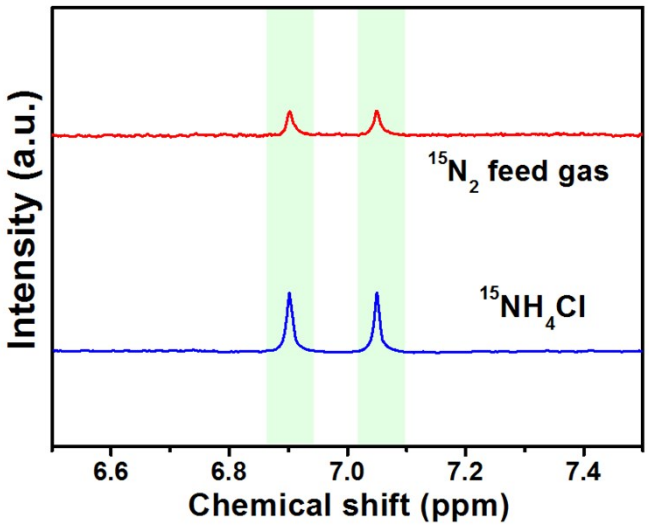

Fig. S8. ^{1}H NMR measurements by using $^{15}N_2$ as feeding gas and $^{15}NH_4Cl$ standard sample.

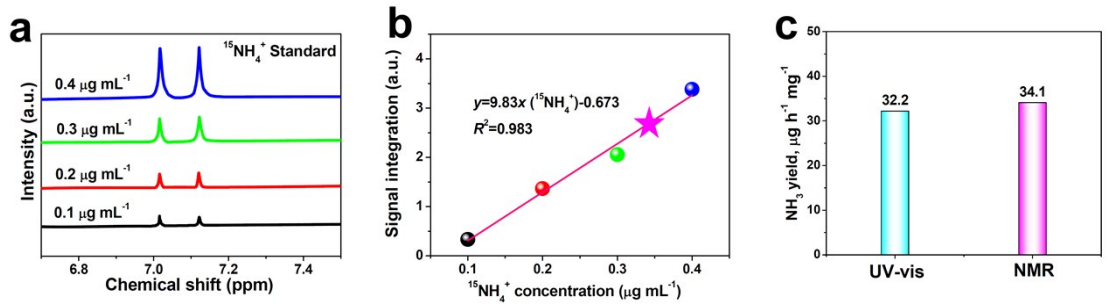

Fig. S9. (a) ^1H NMR spectra of $^{15}NH_4^+$ standard samples with different concentrations, and (b) corresponding calibration curve of $^{15}NH_4^+$ concentration vs. peak area. The pink star represents the $^{15}NH_4^+$ concentration derived from the NRR over $NiFe_2O_4$/RGO for 2 h at -0.5 V. (c) Comparison of the NH_3 yield of $NiFe_2O_4$/RGO obtained from UV-vis and NMR methods.

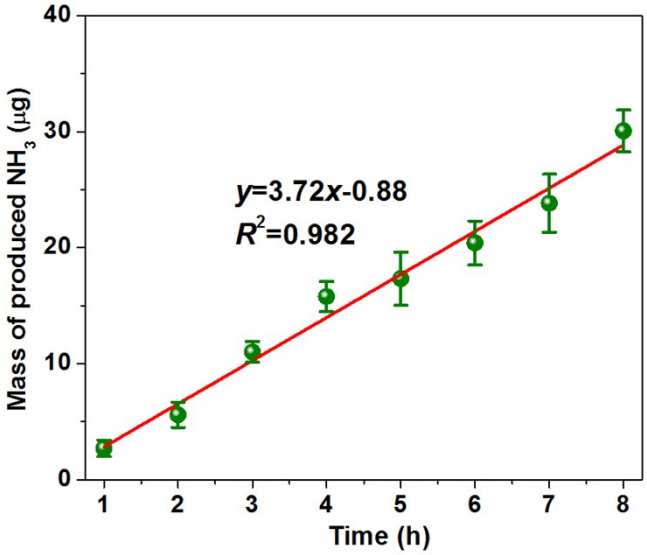

Fig. S10. Mass of produced NH_3 after NRR electrolysis at various times (1-8 h) on $NiFe_2O_4$/RGO at -0.5 V.

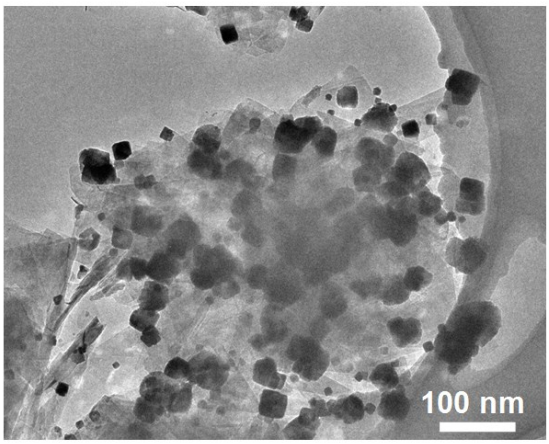

Fig. S11. TEM image of $NiFe_2O_4$/RGO after stability test.

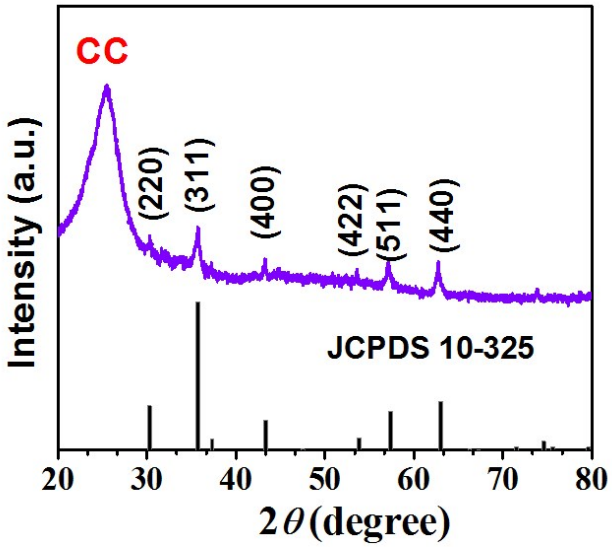

Fig. S12. XRD pattern of $NiFe_2O_4$/RGO after stability test.

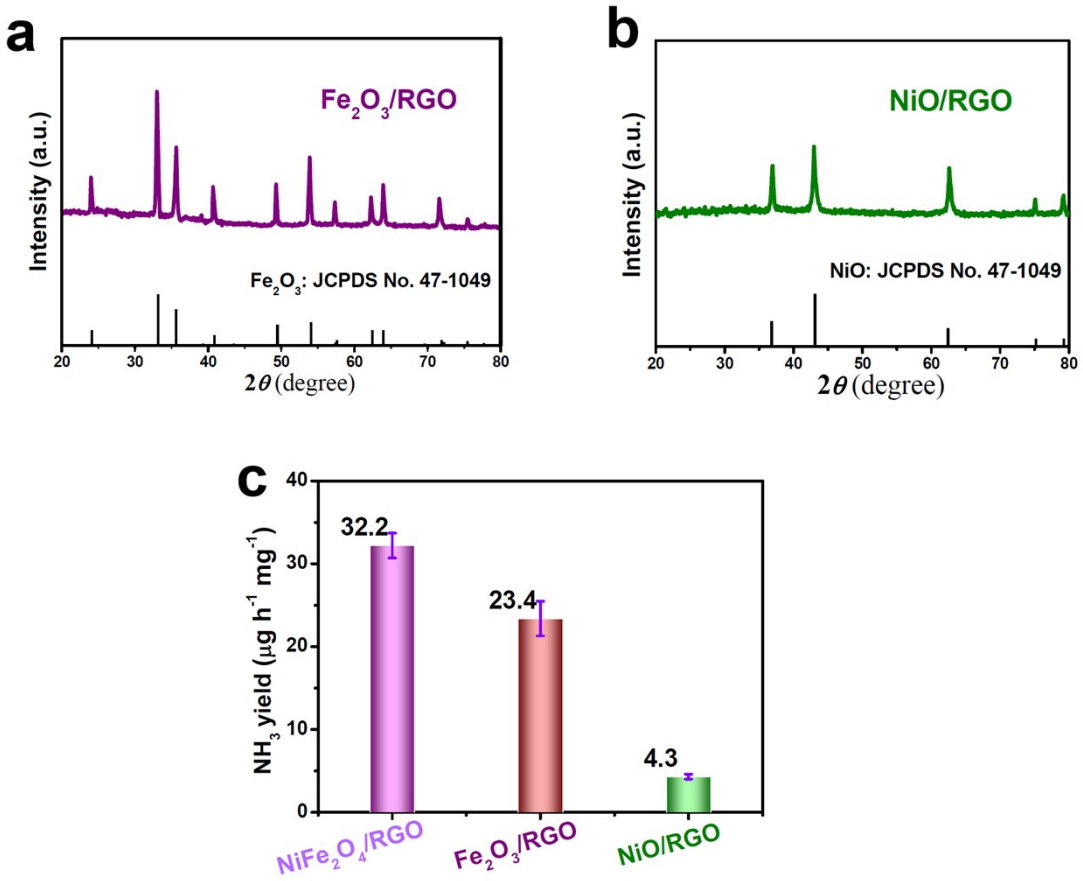

Fig. S13. XRD patterns of (a) Fe_2O_3/RGO (synthesis using the same route as $NiFe_2O_4$/RGO but without addition of $Ni(NO_3)_2 \cdot 6H_2O$) and (b) NiO/RGO (synthesis using the same route as $NiFe_2O_4$/RGO but without addition of $Fe(NO_3)_3 \cdot 9H_2O$). (c) NH_3 yields of $NiFe_2O_4$/RGO, Fe_2O_3/RGO and NiO/RGO after 2 h of NRR electrolysis at -0.5 V.

Table S1. Comparison of optimum NH_3 yield and Faradic efficiency (FE) for recently reported state-of-the-art NRR electrocatalysts at ambient conditions

Catalyst	Electrolyte	Determination method	Optimum Potential (V Vs RHE)	NH_3 yield ($\mu g\ h^{-1}\ mg^{-1}$)	FE (%)	Ref.
Defect-rich MoS_2 nanoflower	0.1 M Na_2SO_4	Indophenol blue method	-0.4	29.28 $\mu g\ h^{-1}\ mg^{-1}$	8.34	[5]
Nb_2O_5 nanofibers	0.1 M HCl	Indophenol blue method	-0.55	43.6 $\mu g\ h^{-1}\ mg^{-1}$	9.26	[6]
Hollow Cr_2O_3 microspheres	0.1 M Na_2SO_4	Indophenol blue method	-0.9	25.3 $\mu g\ h^{-1}\ mg^{-1}$	6.78	[7]
Cubic sub-micron SnO_2 particles	0.1 M Na_2SO_4	Indophenol blue method	-0.7	4.03 $\mu g\ h^{-1}\ mg^{-1}$	2.17	[8]
Au@CeO_2	0.01 M H2SO4	Indophenol blue method	-0.4	28.2 $\mu g\ h^{-1}\ mg^{-1}$	9.5	[9]
Au/CeO_x-RGO	0.1 M KOH	Salicylate method	−0.2	8.31 $\mu g\ h^{-1}\ mg^{-1}$	10.1	[10]
Au-TiO_2 sub-nanocluster	0.1 M HCl	Indophenol blue method	-0.2	21.4 $\mu g\ h^{-1}\ mg^{-1}$	8.11	[11]
Mo_2C/C	0.5 M Li_2SO_4	Nessler's reagent method	-0.3	11.3 $\mu g\ h^{-1}\ mg^{-1}$	7.8	[12]
MXene	0.5 M Li_2SO_4	Nessler's reagent method	-0.1	4.7 $\mu g\ cm^{-2}\ h^{-1}$	5.78	[13]
Fe/Fe_3O_4	0.1 M PBS	Indophenol blue method	-0.3	0.19 $\mu g\ cm^{-2}\ h^{-1}$	8.29	[14]
Spinel Fe_3O_4 nanorods	0.1 M Na_2SO_4	Indophenol blue method	-0.4	5.6×10^{-11} $mol\ s^{-1}\ cm^{-2}$	2.6	[15]
$Bi_4V_2O_{11}$-CeO_2 nanofibers	0.1 M HCl	Indophenol blue method	-0.2	23.21 $\mu g\ h^{-1}\ mg^{-1}$	10.16	[16]
CoP hollow nanocage	1.0 M KOH	Indophenol blue method	-0.4	10.78 $\mu g\ h^{-1}\ mg^{-1}$	7.36	[17]
Mosaic Bi nanosheets	0.1 M Na_2SO_4	Indophenol blue method	-0.8	13.23 $\mu g\ h^{-1}\ mg^{-1}$	10.46	[18]
Mo single atoms	0.1 M KOH	Indophenol blue method (NMR)	-0.3	34 $\mu g\ h^{-1}\ mg^{-1}$	14.6	[19]
$NiFe_2O_4$/RGO	**0.5 M $LiClO_4$**	**Indophenol blue method**	**-0.5**	**32.2 $\mu g\ h^{-1}\ mg^{-1}$**	**9.8**	**This work**

Supplementary references

[1]. D. Zhu, L. Zhang, R. E. Ruther and R. J. Hamers, *Nat. Mater.*, 2013, **12**, 836.

[2]. G. W. Watt and J. D. Chrisp, *Anal. Chem.*, 1952, **24**, 2006-2008.

[3]. B. Hu, M. Hu, L. C. Seefeldt and T. L. Liu, *ACS Energy Lett.*, 2019, **4**, 1053-1054.

[4]. A. A. Peterson, *Energy Environ. Sci.*, 2010, **3**, 1311-1315.

[5]. X. Li, T. Li, Y. Ma, Q. Wei, W. Qiu, H. Guo, X. Shi, P. Zhang, A. M. Asiri and L. Chen, *Adv. Energy. Mater.*, 2018, **8**, 1801357.

[6]. J. Han, Z. Liu, Y. Ma, G. Cui, F. Xie, F. Wang, Y. Wu, S. Gao, Y. Xu and X. Sun, *Nano Energy*, 2018, **52**, 264-270.

[7]. Y. Zhang, W. Qiu, Y. Ma, Y. Luo, Z. Tian, G. Cui, F. Xie, L. Chen, T. Li and X. Sun, *ACS Catal.*, 2018, **8**, 8540-8544.

[8]. L. Zhang, X. Ren, Y. Luo, X. Shi, A. M. Asiri, T. S. Li and X.-P. Sun, *Chem. Commun.*, 2018.

[9]. G. Liu, Z. Cui, M. Han, S. Zhang, C. Zhao, C. Chen, G. Wang and H. Zhang, *Chem. Eur. J.*, 2019, **25**, 5904-5911.

[10]. S. J. Li, D. Bao, M. M. Shi, B. R. Wulan, J. M. Yan and Q. Jiang, *Adv. Mater.*, 2017, **29**, 1700001.

[11]. M. M. Shi, D. Bao, B. R. Wulan, Y. H. Li, Y. F. Zhang, J. M. Yan and Q. Jiang, *Adv. Mater.*, 2017, **29**, 1606550.

[12]. H. Cheng, L. X. Ding, G. F. Chen, L. Zhang, J. Xue and H. Wang, *Adv. Mater.*, 2018, **30**, 1803694.

[13]. Y. R. Luo, G. F. Chen, L. Ding, X. Z. Chen, L. X. Ding and H. H. Wang, *Joule*, 2019, **3**, 279-289.

[14]. L. Hu, A. Khaniya, J. Wang, G. Chen, W. E. Kaden and X. Feng, *ACS Catal.*, 2018, **8**, 9312-9319.

[15]. Q. Liu, X. Zhang, B. Zhang, Y. Luo, G. Cui, F. Xie and X. Sun, *Nanoscale*, 2018, **10**, 14386-14389.

[16]. C. Lv, C. Yan, G. Chen, Y. Ding, J. Sun, Y. Zhou and G. Yu, *Angew. Chem. Int. Edit.*, 2018, **130**, 6181-6184.

[17]. W. Guo, Z. Liang, J. Zhao, B. Zhu, K. Cai, R. Zou and Q. Xu, *Small Methods*, 2018, **2**, 1800204.

[18]. L. Li, C. Tang, B. Xia, H. Jin, Y. Zheng and S.-Z. Qiao, *ACS Catal.*, 2019, **9**, 2902-2908.

[19]. L. Han, X. Liu, J. Chen, R. Lin, H. Liu, F. Lu, S. Bak, Z. Liang, S. Zhao and E. Stavitski, *Angew. Chem. Int. Edit.*, 2018, **58**, 2321-2325.